

Heat and Mass Transfer of a Non-Newtonian Fluid Flow in an Anisotropic Porous Channel with Chemical Surface Reaction

Z. Neffah¹, H. Kahalerras^{1,*} and B. Fersadou¹

Abstract: A numerical study of heat and mass transfer in a non-Newtonian fluid in a parallel-plate channel partly filled with an anisotropic porous medium and subjected to an exothermic chemical reaction on its walls has been conducted. The flow field in the porous region has been modeled by the modified Brinkman-Forchheimer extended Darcy model for power-law fluids and a finite volume method has been used to solve the governing equations. The influence played by a variation of the anisotropic ratio on thermal conductivity, power-law index, Darcy number, and chemical reaction characteristics has been examined. We show that the anisotropy of a porous medium can lead to significant improvements in terms of heat and mass transfer with respect to the isotropic case. The shear-thickening fluids exhibit the highest values of mean Nusselt and Sherwood numbers at large Darcy number. Finally, we show that an increase in the chemical reaction parameters leads to a reduction of the heat and mass transfer rates.

Keywords: Heat and mass transfer, non-Newtonian fluid, anisotropic porous medium, chemical reaction.

Nomenclature

c	Concentration (mol.m^{-3})
C	Inertial coefficient
C^*	Modified inertial coefficient
C_p	Specific heat at constant pressure ($\text{J.kg}^{-1}. \text{K}^{-1}$)
D	Mass diffusivity ($\text{m}^2. \text{s}^{-1}$)
Da	Darcy number
D_m	Modified Damköhler number
e_p	Porous medium thickness (m)
E	Activation energy (J.mol^{-1})
FK_m	Modified Frank- Kamenetskii number
H	Channel width (m)
k	Thermal conductivity ($\text{W.m}^{-1}. \text{K}^{-1}$)
k_0	Pre-exponential factor of Arrhenius (s^{-1})
K	Intrinsic permeability of the porous medium (m^2)
K^*	Modified permeability of the porous medium (m^{n+1})

¹ Faculty of Mechanical and Process Engineering, Houari Boumediene University of Sciences and Technology (USTHB), B. P. 32, El Alia, Bab Ezzouar 16111, Algiers-Algeria.

* Corresponding author: H. Kahalerras. Email: hkahalerras@usthb.dz.

ℓ	Channel length (m)
Le	Lewis number
n	Power-law index
Nu	Nusselt number
p	Pressure (Pa)
Pr	Prandtl number
Q	Heat of reaction ($\text{J}\cdot\text{mol}^{-1}$)
R	Universal gas constant ($\text{J}\cdot\text{mol}^{-1}\cdot\text{K}^{-1}$)
Re	Reynolds number
R_k	Thermal conductivity ratio
R_μ	Viscosity ratio
Sh	Sherwood number
T	Temperature (K)
u	Axial velocity ($\text{m}\cdot\text{s}^{-1}$)
v	Transverse velocity ($\text{m}\cdot\text{s}^{-1}$)
x	Axial coordinate (m)
y	Transverse coordinate (m)

Greek symbols

γ	Activation energy parameter
ε	Porosity
η	Apparent viscosity ($\text{Pa}\cdot\text{s}$)
θ	Dimensionless temperature
λ	Anisotropic thermal conductivity ratio
μ^*	Consistency factor ($\text{Pa}\cdot\text{s}^n$)
ρ	Density ($\text{kg}\cdot\text{m}^{-3}$)
τ	Shear stress (Pa)

Subscripts

e	Effective
i	Inlet
m	Mean
w	Wall

1 Introduction

In most of the work carried out over the past years, the porous medium was considered to be homogeneous and isotropic, but in many practical applications these materials are anisotropic in their mechanical and thermal properties. Anisotropy, which is generally a result of preferential orientation of the grains or fibers, is encountered in many natural and industrial systems such as fibrous materials, sedimentary soils, rock formation, drying of food grains, rod bundles in a nuclear reactor core, thermal insulation, heat exchanger tubes, etc. Chang et al. [Chang and Hsiao (1993); Jingzhou and Ranqia (1996)] by studying the problem of natural convection in enclosures filled with anisotropic porous media, found that permeability and thermal conductivity ratios have

opposing effects on the heat transfer rate. Using a semi-implicit procedure and the Galerkin finite element method, Nithiarasu et al. [Nithiarasu, Sujatha, Ravindran et al. (2000)] examined the effect of a hydrodynamically and thermally anisotropic porous medium on non-Darcy natural convection. Govender [Govender (2006)] investigated analytically the problem of natural convection in a rotating anisotropic porous layer. He found that the convection is stabilized when the thermal anisotropy ratio, which depends on both thermal and mechanical anisotropy parameters, increases. The influence of viscous dissipation on forced convection heat transfer in an anisotropic porous channel with oblique principal axes was analyzed analytically by Mobedi et al. [Mobedi, Cekmer and Pop (2010)]. A directional permeability parameter A^* was introduced to combine both the effect of the permeability ratio and angle orientation. Simulation of two-phase flows in anisotropic porous media was conducted by Negara et al. [Negara, Salama and Sun (2015)] using multipoint flux approximation.

In several industries which contain porous media, the fluids involved may exhibit non-Newtonian flow behavior. Examples of engineering applications are enhanced oil recovery, food technology, materials processing, filtration processing, packed bed reactors, geothermal engineering, insulation system, and many others. Thus, a growing number of researchers have been attracted by this topic. An analysis of non-Darcy forced convection in a parallel-plate channel filled with a porous medium saturated by a non-Newtonian inelastic fluid was investigated by Nakayama et al. [Nakayama and Shenoy (1993)] in order to obtain an explicit formula for the fully developed Nusselt number. Chen et al. [Chen and Hadim (1998)] performed a numerical study of forced convection flow in a porous channel saturated by a power-law fluid. In the non-Darcy regime, they obtained an augmentation of heat transfer rate and a reduction of pressure drop with the decrease of the power-law index. The impact of macroscopic inertial term on transient flow of a non-Newtonian fluid in parallel-plate channels completely filled with porous medium was considered by Al-Nimr et al. [Al-Nimr and Aldoss (2004)]. Nebbali et al. [Nebbali and Bouhadeb (2006)] analyzed numerically the forced convective flow of a power-law fluid in a 3D square duct partially filled with a porous medium. It was demonstrated that shear-thickening fluids exhibit the highest rates of heat transfer and pressure drop. A gray lattice Boltzmann model was used by Chen et al. [Chen, Cao and Zhu (2009)] to study the flow of a power-law fluid through a parallel plate channel partly filled with a porous substrate. The results show that the slip velocity at porous interface increases with power-law index and porosity of the porous media. Chen et al. [Chen and Tso (2011)] considered the forced convective heat transfer in a channel embedded in a power-law fluid saturated porous medium and made comparisons with Newtonian fluid concerning the effects of viscous dissipation for various values of Darcy number. Alsabery et al. [Alsabery, Chamkha, Hussain et al. (2015)] used the heatline technique to visualize the natural convection in an inclined trapezoidal cavity partly filled with a nanofluid porous layer and partly with a non-Newtonian fluid.

Considerable attention has also been given to the topic of simultaneous heat and mass transfer in reactive porous media due to their wide applications in nature and engineering practice such as catalytic and nuclear reactors, geothermal and petroleum reservoirs, oil delivery and so on. In these processes the chemical reaction may either occur uniformly

throughout a given phase (homogeneous reaction) or in a restricted region (boundary) of the phase (heterogeneous reaction). Minto et al. [Minto, Ingham and Pop (1998)] considered a theoretical analysis of steady free convection along a vertical surface embedded in a fluid-saturated porous medium, where the flow is driven by a catalytic surface heating. Li et al. [Li, Wu, Tian et al. (2007)] developed a non-thermal equilibrium model to study the coupled heat and mass transfer in a porous medium undergoing a strong endothermic chemical reaction. The onset of convection in a horizontal porous layer with an exothermic surface reaction, described by the Arrhenius kinetics, on lower wall has been considered by Postelnicu [Postelnicu (2009)]. Bousri et al. [Bousri, Bouhadeif, Langlat et al. (2011)] carried out a numerical analysis of coupled heat and mass transfer in a cylindrical duct filled with a reactive porous medium by considering the existence of a non thermal equilibrium between the solid and fluid phases. In their paper, Matin et al. [Matin and Pop (2013)] presented an exact solution for the problem of fully developed forced convection in a porous channel filled with a nanofluid and subjected to constant heat flux and first order catalytic reaction on the walls. An analytical solution has been obtained by Moshizi [Moshizi (2015)] for convective heat and mass transfer characteristics of Cu-water nanofluid inside a porous microchannel in the presence of a uniform magnetic field and chemical reaction on the walls. Recently, Amini et al. [Amini, Kafrudi, Habibi et al. (2017)] used a magnetite nanofluid (Fe_3O_4 -water) in a stagnation flow influenced by chemical reaction and magnetic field.

The aim of this paper is to simulate heat and mass transfer of non-Newtonian power-law fluid flow in a channel partly filled with an anisotropic porous medium when an exothermic and non-isothermal chemical reaction, governed by Arrhenius kinetics, takes place on its walls. A parametric study is conducted to examine the effects of the anisotropic thermal conductivity ratio, power-law index, Darcy number, as well as the characteristics of chemical reaction.

2 Mathematical formulation

The physical model, shown in Fig. 1, consists of a two-dimensional parallel-plate channel partly filled with an anisotropic porous medium of thickness e_p and porosity ε . The non-Newtonian fluid enters the channel with a constant velocity U_i and uniform temperature T_i and species concentration C_i . An exothermic surface reaction is taking place on the walls, and can be represented by a single first-order, non-isothermal and one-step reaction governed by Arrhenius kinetics.

The forced convection flow is assumed to be steady, two-dimensional, laminar and incompressible with no heat generation and neglecting viscous dissipation. The thermophysical properties of the fluid are assumed to be constant except for the viscosity of the power-law fluid which depends on the shear rate. The porous medium is considered homogeneous, anisotropic in thermal conductivity and saturated with single phase non-Newtonian fluid which is in local equilibrium with the solid matrix.

The fluid flow in the porous medium is described by the modified Brinkman-Forchheimer extended Darcy model for power-law fluids to incorporate the viscous and inertia effects as reported by Shenoy [Shenoy (1994)]. The continuity, momentum, energy and concentration governing equations are written as follows:

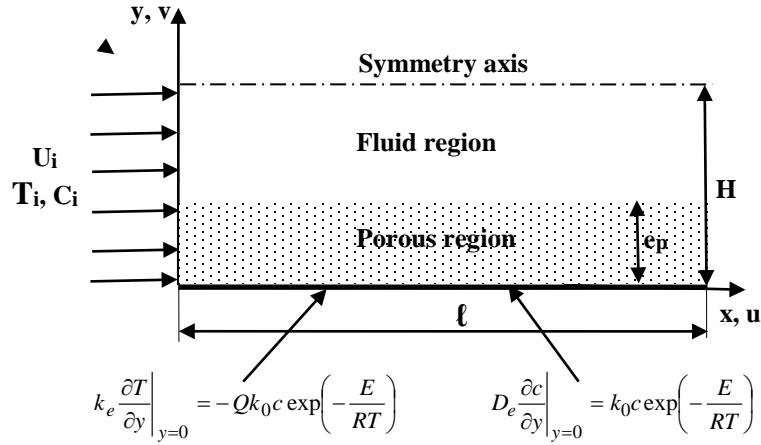


Figure 1: Physical domain

Continuity

$$\frac{\partial u}{\partial x} + \frac{\partial v}{\partial y} = 0 \quad (1)$$

Momentum

$$\frac{\rho}{\varepsilon^2} \left(u \frac{\partial u}{\partial x} + v \frac{\partial u}{\partial y} \right) = -\frac{\partial p}{\partial x} + \frac{1}{\varepsilon^n} \frac{\partial \tau_{xx}}{\partial x} + \frac{1}{\varepsilon^n} \frac{\partial \tau_{xy}}{\partial y} - \frac{\mu^*}{K^*} |\vec{V}|^{n-1} u - \rho \frac{C}{\sqrt{K}} |\vec{V}| u \quad (2)$$

$$\frac{\rho}{\varepsilon^2} \left(u \frac{\partial v}{\partial x} + v \frac{\partial v}{\partial y} \right) = -\frac{\partial p}{\partial y} + \frac{1}{\varepsilon^n} \frac{\partial \tau_{yy}}{\partial y} + \frac{1}{\varepsilon^n} \frac{\partial \tau_{yx}}{\partial x} - \frac{\mu^*}{K^*} |\vec{V}|^{n-1} v - \rho \frac{C}{\sqrt{K}} |\vec{V}| v \quad (3)$$

Energy

$$\rho C_p \left(u \frac{\partial T}{\partial x} + v \frac{\partial T}{\partial y} \right) = \frac{\partial}{\partial x} \left(k_{ex} \frac{\partial T}{\partial x} \right) + \frac{\partial}{\partial y} \left(k_{ey} \frac{\partial T}{\partial y} \right) \quad (4)$$

Concentration

$$u \frac{\partial c}{\partial x} + v \frac{\partial c}{\partial y} = D_e \left(\frac{\partial^2 c}{\partial x^2} + \frac{\partial^2 c}{\partial y^2} \right) \quad (5)$$

where $|\vec{V}| = \sqrt{u^2 + v^2}$, K^* the modified permeability of the power-law fluid, k_{ex} and k_{ey} the effective thermal conductivity of the porous medium in the axial direction and transverse direction respectively and $D_e = \varepsilon D$.

The components of the shear stress tensor are:

$$\tau_{xx} = 2\eta \frac{\partial u}{\partial x}, \tau_{yy} = 2\eta \frac{\partial v}{\partial y}, \tau_{xy} = \tau_{yx} = \eta \left(\frac{\partial v}{\partial x} + \frac{\partial u}{\partial y} \right) \quad (6)$$

For a power-law fluid, the expression of the apparent viscosity is given by:

$$\eta = \mu^* \left[2 \left(\frac{\partial u}{\partial x} \right)^2 + 2 \left(\frac{\partial v}{\partial y} \right)^2 + \left(\frac{\partial u}{\partial y} + \frac{\partial v}{\partial x} \right)^2 \right]^{\frac{n-1}{2}} \quad (7)$$

where μ^* is the consistency factor of the power-law fluid. In the non porous region: $\varepsilon = 1$, $k_e = k$, $D_e = D$, $K \rightarrow \infty$, and $K^* \rightarrow \infty$.

The associated boundary conditions are:

$$x=0: u=U_i, v=0, T=T_i, c=C_i \quad (8)$$

$$x=l: \frac{\partial u}{\partial x} = 0, v=0, \frac{\partial T}{\partial x} = 0, \frac{\partial c}{\partial x} = 0 \quad (9)$$

$$y=0: u=0, v=0, k_{ey} \frac{\partial T}{\partial y} \Big|_{y=0} = -Qk_0c \exp\left(-\frac{E}{RT}\right), D_e \frac{\partial c}{\partial y} \Big|_{y=0} = k_0c \exp\left(-\frac{E}{RT}\right) \quad (10)$$

$$y=H: \frac{\partial u}{\partial y} = 0, v=0, \frac{\partial T}{\partial y} = 0, \frac{\partial c}{\partial y} = 0 \quad (11)$$

At porous-fluid interface: continuity of pressure, velocity components, stresses, temperature, concentration and heat and mass fluxes. To ensure these conditions, the harmonic mean formulation suggested by Patankar [Patankar (1980)] is used to handle the abrupt changes in the thermophysical properties between clear fluid and porous media.

Using the dimensionless quantities:

$$X = \frac{x}{H}; Y = \frac{y}{H}; U = \frac{u}{\varepsilon U_i}; V = \frac{v}{\varepsilon U_i}; P = \frac{p}{\rho U_i^2}; \theta = \frac{T - T_i}{RT_i^2/E}; C = \frac{c}{C_i}$$

the governing Eqs. (1-5) and boundary conditions (8-11) become:

$$\frac{\partial U}{\partial X} + \frac{\partial V}{\partial X} = 0 \quad (12)$$

$$U \frac{\partial U}{\partial X} + V \frac{\partial V}{\partial Y} = -\frac{\partial P}{\partial X} + \frac{\partial}{\partial X} \left[2 \frac{\Phi}{\text{Re}} \frac{\partial U}{\partial X} \right] + \frac{\partial}{\partial Y} \left[\frac{\Phi}{\text{Re}} \left(\frac{\partial U}{\partial Y} + \frac{\partial V}{\partial X} \right) \right] - \frac{1}{\text{Re Da}^{\frac{n+1}{2}}} |\vec{V}|^{n-1} U - \frac{C^*}{\sqrt{\text{Da}}} |\vec{V}| U \quad (13)$$

$$U \frac{\partial V}{\partial X} + V \frac{\partial V}{\partial Y} = -\frac{\partial P}{\partial Y} + \frac{\partial}{\partial Y} \left[2 \frac{\Phi}{\text{Re}} \frac{\partial V}{\partial Y} \right] + \frac{\partial}{\partial X} \left[\frac{\Phi}{\text{Re}} \left(\frac{\partial V}{\partial X} + \frac{\partial U}{\partial Y} \right) \right] - \frac{1}{\text{Re Da}^2} |\bar{V}|^{n-1} V - \frac{C^*}{\sqrt{\text{Da}}} |\bar{V}| V \quad (14)$$

$$U \frac{\partial \theta}{\partial X} + V \frac{\partial \theta}{\partial Y} = \frac{R_k}{\varepsilon \text{Pr Re}} \left(\frac{\partial^2 \theta}{\partial X^2} + \lambda \frac{\partial^2 \theta}{\partial Y^2} \right) \quad (15)$$

$$U \frac{\partial C}{\partial X} + V \frac{\partial C}{\partial Y} = \frac{1}{\text{Le Pr Re}} \left(\frac{\partial^2 C}{\partial X^2} + \frac{\partial^2 C}{\partial Y^2} \right) \quad (16)$$

$$X=0: U=1, V=0, \theta=0, C=1 \quad (17)$$

$$X=L: \frac{\partial U}{\partial X} = 0, V=0, \frac{\partial \theta}{\partial X} = 0, \frac{\partial C}{\partial X} = 0 \quad (18)$$

$$Y=0: U=0, V=0, \frac{\partial \theta}{\partial Y} \Big|_{Y=0} = -\frac{\text{FK}_m}{\lambda} C \exp\left(\frac{\theta}{\gamma\theta+1}\right), \frac{\partial C}{\partial Y} \Big|_{Y=0} = D_m C \exp\left(\frac{\theta}{\gamma\theta+1}\right) \quad (19)$$

$$Y=1: \frac{\partial U}{\partial Y} = 0, V=0, \frac{\partial \theta}{\partial Y} = 0, \frac{\partial C}{\partial Y} = 0 \quad (20)$$

The dimensionless parameters appearing in the governing equations and boundary conditions are defined as follows:

$$\text{Re} = \frac{\rho H^n U_i^{2-n}}{\mu^*}, \text{Da} = \frac{\left(\frac{K^*}{\varepsilon^n}\right)^{\frac{2}{n+1}}}{H^2}, C^* = C \frac{\left(\frac{K^*}{\varepsilon^n}\right)^{\frac{1}{n+1}} \varepsilon^2}{K^{1/2} \varepsilon^{\frac{n}{n+1}}}, \text{Pr} = \frac{\mu^* C_p}{k} \left(\frac{U_i}{H}\right)^{n-1}, R_k = \frac{k_{\text{ex}}}{k}$$

$$\lambda = \frac{k_{\text{ey}}}{k_{\text{ex}}}, \text{Le} = \frac{k}{\rho C_p D}, \text{FK}_m = \frac{Q k_0 C_1 H}{k_{\text{ex}} RT_1^2} \exp\left(-\frac{1}{\gamma}\right), D_m = \frac{k_0 H}{D_e} \exp\left(-\frac{1}{\gamma}\right), \gamma = \frac{RT_i}{E}$$

$$\Phi = \left[2 \left(\frac{\partial U}{\partial X} \right)^2 + 2 \left(\frac{\partial V}{\partial Y} \right)^2 + \left(\frac{\partial U}{\partial Y} + \frac{\partial V}{\partial X} \right)^2 \right]^{\frac{n-1}{2}}$$

The local Nusselt and Sherwood numbers along the upper wall of the channel are evaluated as:

$$\text{Nu} = -\lambda R_k \frac{\frac{\partial \theta}{\partial Y} \Big|_{Y=0}}{\theta_w - \theta_m} \quad \text{and} \quad \text{Sh} = -\varepsilon \frac{\frac{\partial C}{\partial Y} \Big|_{Y=0}}{C_w - C_m} \quad (21)$$

Where the mean temperature θ_m and mean concentration C_m are calculated as follows:

$$\theta_m = \frac{\int_0^1 U \theta dY}{\int_0^1 U dY} \quad \text{and} \quad C_m = \frac{\int_0^1 U C dY}{\int_0^1 U dY} \quad (22)$$

The average Nusselt and Sherwood numbers are defined as:

$$\text{Nu}_m = \frac{1}{L} \int_0^L \text{Nu} dX \quad \text{and} \quad \text{Sh}_m = \frac{1}{L} \int_0^L \text{Sh} dX \quad (23)$$

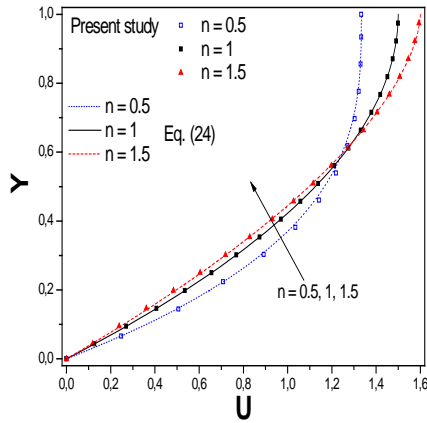
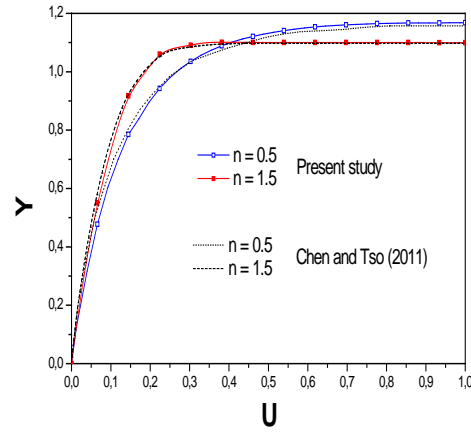
3 Numerical procedure

The finite volume method is used to solve the governing equations using a pressure-velocity formulation. A staggered grid is considered such that velocity components are located at the control volume faces, whereas pressure, temperature and concentration are located at the centers as suggested by Patankar [Patankar (1980)]. The power law scheme is employed in the discretizing procedure to treat the convection and diffusion terms. In the momentum equations, the source terms related to the porous medium was linearized as suggested by Patankar [Patankar (1980)]. For the terms associated to the non-Newtonian behavior of the fluid, first order forward difference and second order central finite difference were used. The obtained algebraic equations are solved using the line by line technique, combining between the tridiagonal matrix algorithm and the Gauss-Seidel method. A non-uniform grid is employed in the transverse direction by locating the finer meshes near the axis of symmetry, the porous-fluid interface and the lower wall of the channel. To analyze the effect of the grid size on the numerical solution, several grid systems are tested for various combinations of the controlling parameters. A typical test is shown in Tab. 1 and a grid system of 250×50 (in X and Y directions, respectively) is adopted since the relative errors on the mean Nusselt and Sherwood numbers are less than 0.1%. For the convergence criteria of the iterative process, the relative variations of velocity components, temperature and concentration between two successive iterations are required to be smaller than 10^{-6} . As the simulation time and the error evolve in opposite directions; so trial calculations were necessary to optimize the computation time and accuracy. The elaborated computational code is validated by comparing the developed velocity profile at the channel exit for different values of the power-law index with two limiting cases available in the literature. The first comparison is made with the analytical solution (Eq. (24)) given by Nebbali et al. [Nebbali and Bouhadeb (2011)], whereas the second one concerns the numerical solution obtained by Chen et al. [Chen and Tso (2011)] in a porous channel using the Brinkman extended Darcy's law. Fig. 2a and Fig. 2b show a very good agreement.

$$U(Y) = \frac{2n+1}{n+1} \left[1 - (1-Y)^{\frac{n+1}{n}} \right] \quad (24)$$

Table 1: Grid sensitivity analysis for for $n=1.5$, $Da=10^{-2}$, $\lambda=10$, $FK_m=1$ and $D_m=5$

Grid number ($X \times Y$)	100×10	150×20	200×30	250×50	300×60
Nu_m	20.962	20.030	19.898	19.814	19.806
Relative error (%)	-	4.45	0.66	0.42	0.04
Sh_m	2.031	1.940	1.927	1.918	1.917
Relative error (%)	-	4.48	0.67	0.47	0.05

**Figure 2a:** Developed velocity profiles for various values of n , $Da \rightarrow \infty$ and $\varepsilon=1$ **Figure 2b:** Developed velocity profiles for various values of n , $Da=10^{-2}$ and $C^*=0$

4 Results

Due to the great number of parameters, few of them are kept constant. The numerical calculations are performed for a thickness $E_p=0.4$, a porosity $\varepsilon=0.95$, an inertia coefficient $C^*=0.1$, a Prandtl number $Pr=10$, a Reynolds number $Re=100$, a Lewis number $Le=1$, a viscosity ratio $R_\mu=1$ and a thermal conductivity ratio $R_k=1$. The results obtained by varying the activation energy parameter γ from 0.01 to 100 showed that its effect is negligible. So, its value is set to 0.1. The results concerning the thermal and mass fields will be decomposed principally into two parts. At first, will be discussed the effect of the porous medium anisotropy described by the anisotropic thermal conductivity ratio ($\lambda=0.1, 1$ and 10) for different values of Darcy number ($10^{-6} \leq Da \leq 1$) and power-law index characterizing the non-Newtonian behavior of the fluid ($n=0.5, 1$ and 1.5). The second part will be devoted to the study of the influence of chemical reaction characteristics ($0.1 \leq FK_m \leq 20$ and $5 \leq D_m \leq 80$). The results will be presented in terms of velocity, temperature and concentration distributions, and in terms of heat and mass transfer coefficients described by the Nusselt and Sherwood numbers respectively.

The streamwise velocity profiles at the channel exit for different values of the power-law index n at $Da=10^{-3}$ are depicted in Fig. 3 where it appears that the presence of a porous layer of finite thickness tends to slowdown the fluid motion which escapes to the

nonporous region offering less resistance to the flow. The rheological properties of the fluid seem to affect slightly the velocity in the porous layer with however the highest resistance to the flow obtained with the shear-thinning fluid ($n=0.5$). This behavior, reversed by moving away from the porous-fluid interface, is found again by approaching the symmetry axis where the velocity is maximum whatever the value of the power-index law and is the largest for the shear-thickening fluid ($n=1.5$).

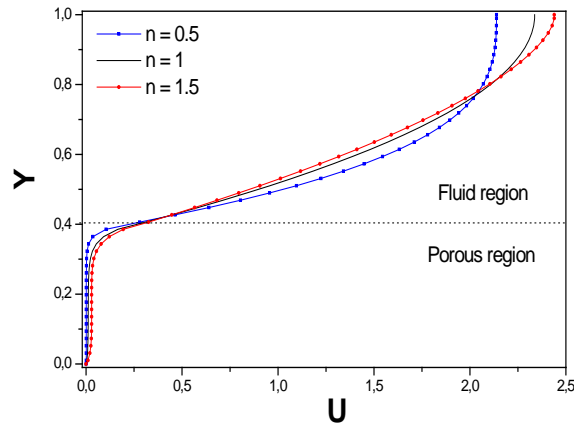


Figure 3: Velocity profiles at the channel exit for various values of n and $Da=10^{-3}$

Fig. 4a, depicting the temperature and concentration profiles at the channel exit for various non-Newtonian fluids, reveals opposing trends for θ and C where the highest temperatures are localized near the walls seat of an exothermic chemical reaction whose effect decreases by going towards the channel center where the temperature approaches that of the fluid at the channel inlet, and vice versa for the concentration. The rheological properties of the fluid influence slightly the temperature and concentration, with however moderately higher and lower values respectively when the fluid is shear-thinning ($n=0.5$). For a thermally anisotropic porous medium (Fig. 4b), values of λ lower than unity correspond to an effective thermal conductivity in the transverse direction k_{ey} lower than that in the axial direction k_{ex} which is constant since $R_k=k_{ex}/k=1$. This will reduce heat transfer since the heat generated by the chemical reaction will not be evacuated and large values of temperature are obtained which will accelerates the reaction and allow the consumption of reagents.

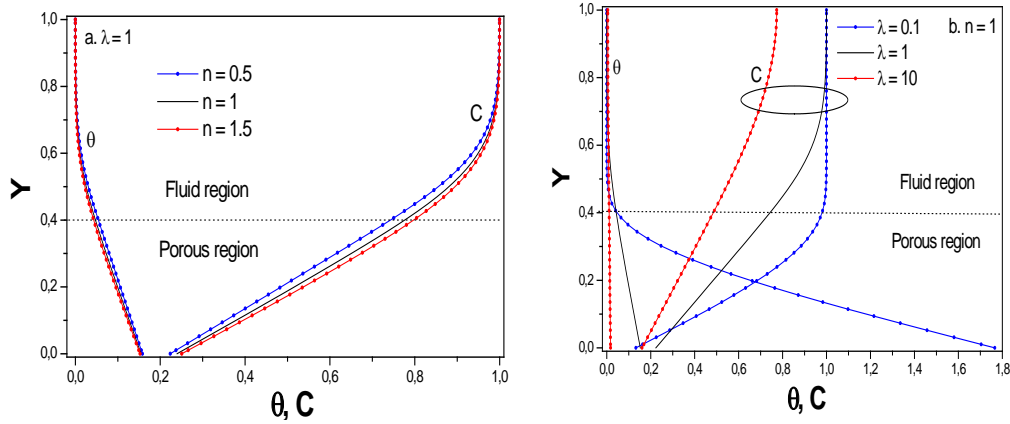


Figure 4: Temperature and concentration profiles at the channel exit for various values of n and λ : $Da=10^{-3}$, $FK_m=1$ and $D_m=5$

The evolutions of the mean Nusselt and Sherwood numbers with λ and n are presented in Fig. 5. The heat transfer is enhanced by the increase of the effective thermal conductivity in the transverse direction Y ($\lambda = k_{ey}/k_{ex}$ with k_{ex} fixed because $R_k=1$). This situation will lead to a decrease of the fluid temperature and an increase of its concentration in the vicinity of the channel walls (Fig. 4b), causing a reduction of mass transfer and then a diminution of Sh_m with λ . Concerning the influence of the power-law index, it appears that the heat and mass transfers are improved with the augmentation of the value of n with the reduction of the difference between the various types of fluids for highly thermally anisotropic porous media.

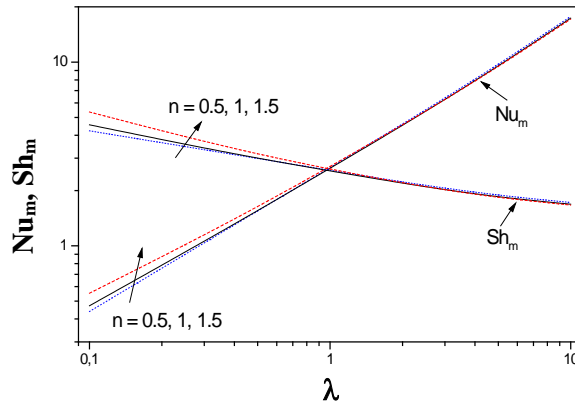


Figure 5: Variation of Nu_m and Sh_m with λ : $Da=10^{-3}$, $FK_m=1$ and $D_m=5$

Whether the porous medium is isotropic or anisotropic and the fluid Newtonian or non-Newtonian, it appears from Fig. 6 that there is an increase of heat and mass transfer with the Darcy number. This result for the partly porous channel has been widely found in the literature [Chikh, Boumedien, Bouhadef et al. (1995); Nebbali and Bouhadef (2006)]. For porous media with low anisotropic ratio ($\lambda=0.1$), the type of fluid seems to have almost

no effect on the values of Nu_m and Sh_m until $Da \approx 10^{-4}$ beyond which the shear-thickening fluid ($n=1.5$) leads to the higher performances of the system. However, this result is not reproduced for all the anisotropy situations of the porous medium where the transfer rates achieved with the shear thickening fluid exceed those obtained with shear-thinning fluid ($n=0.5$) only from a given permeability whose value is strongly related to λ ($Da \approx 6 \times 10^{-4}$ for $\lambda=1$ and $Da \approx 3 \times 10^{-3}$ for $\lambda=10$).

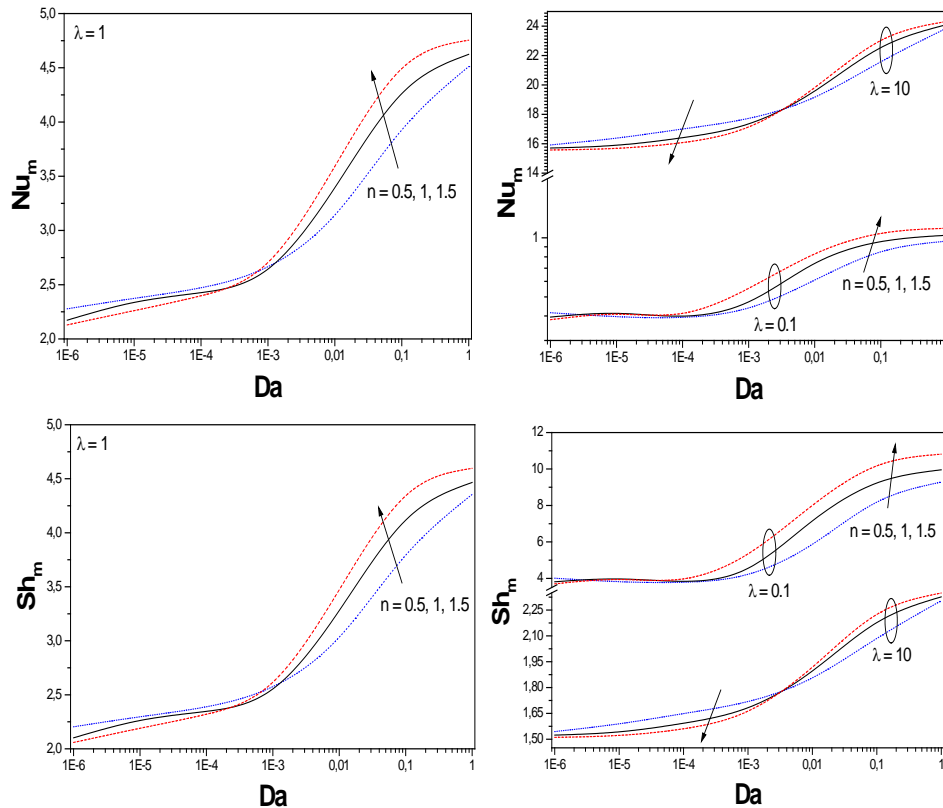


Figure 6: Variation of Nu_m and Sh_m with Da : $FK_m=1$ and $D_m=5$

To highlight the effect of the porous medium anisotropy on heat and mass transfer, we illustrate on Fig. 7 the evolution of the ratios R_{Nu_m} and R_{Sh_m} , normalized by the values of Nu_m and Sh_m of the isotropic case ($\lambda=1$), with the Darcy number. R_{Nu_m} and R_{Sh_m} increase for $\lambda=0.1$, decrease for $\lambda=10$ and finally reach constants values at large permeabilities. Gains on heat and mass transfer are obtained for $\lambda=10$ and $\lambda=0.1$ respectively, with maximum values around 620% for Nu_m at $Da=10^{-6}$ and about 120% for Sh_m at $Da=1$. The situation is reversed for heat and mass losses with $(R_{Nu_m})_{min} \approx 0.16$ and $(R_{Sh_m})_{min} \approx 0.50$. The shear-thinning fluid leads to the highest heat transfer gains and losses, while the lowest values are reached with the shear-thickening fluid, and vice versa for the mass transfer.

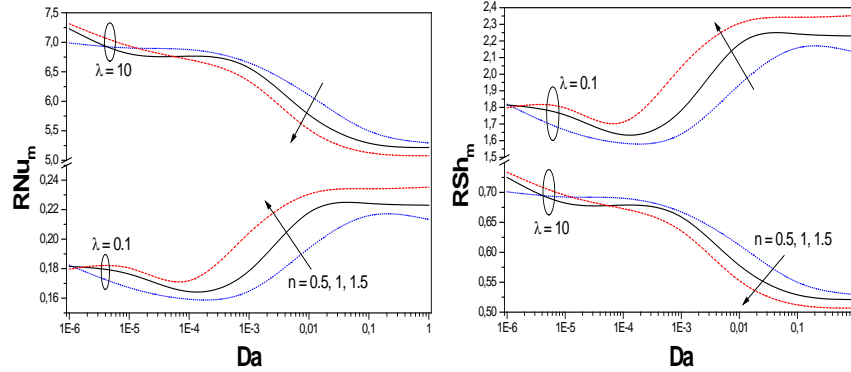


Figure 7: Variation of RNu_m and RSh_m with Da : $FK_m=1$ and $D_m=5$

To study the impact of the parameters characterizing the chemical reaction on heat and mass transfer, an isotropic porous medium ($\lambda=1$) will be considered thereafter, knowing that similar results were found when anisotropy was taken into account.

The influence of the modified Frank-Kamenetskii number on the parietal and mean temperatures and concentrations for different values of the power-law index is illustrated on Fig. 8. It appears from this figure that the shape of the parietal temperature curves is initially growing along the channel before it reaches a constant value. This behavior is due to the exothermic nature of the chemical reaction that increases the temperature until a maximum value corresponding to the most predominant effect of this reaction. Beyond this peak, the temperature is controlled by the transport. As the reaction occurs on the surface of the channel walls and give rise to heat generation, its temperature increases significantly with the Frank-Kamenetskii number. Indeed, this parameter translates directly the influence of the reaction on the heat exchange; more FK_m is important more the heat release by the exothermic reaction is higher, thereby causing an increase of θ_w . In contrast to the wall temperature, the curves of the parietal concentration present a rather decreasing shape from the channel entrance to tend towards the establishment of the regime also. The effect of FK_m is nevertheless similar insofar as for the temperature, its increase reduces C_w and accelerates the establishment. Indeed, at high values of Frank-Kamenetskii number the majority of the reactants are transformed into products and so concentration decreases towards zero. The same behavior is found for the mean temperature θ_m and mean concentration C_m with however a widely lower magnitude and disappearance of the establishment. The impact of the power-law index is only apparent in the region near the channel entrance and at low values of FK_m with however a similar behavior.

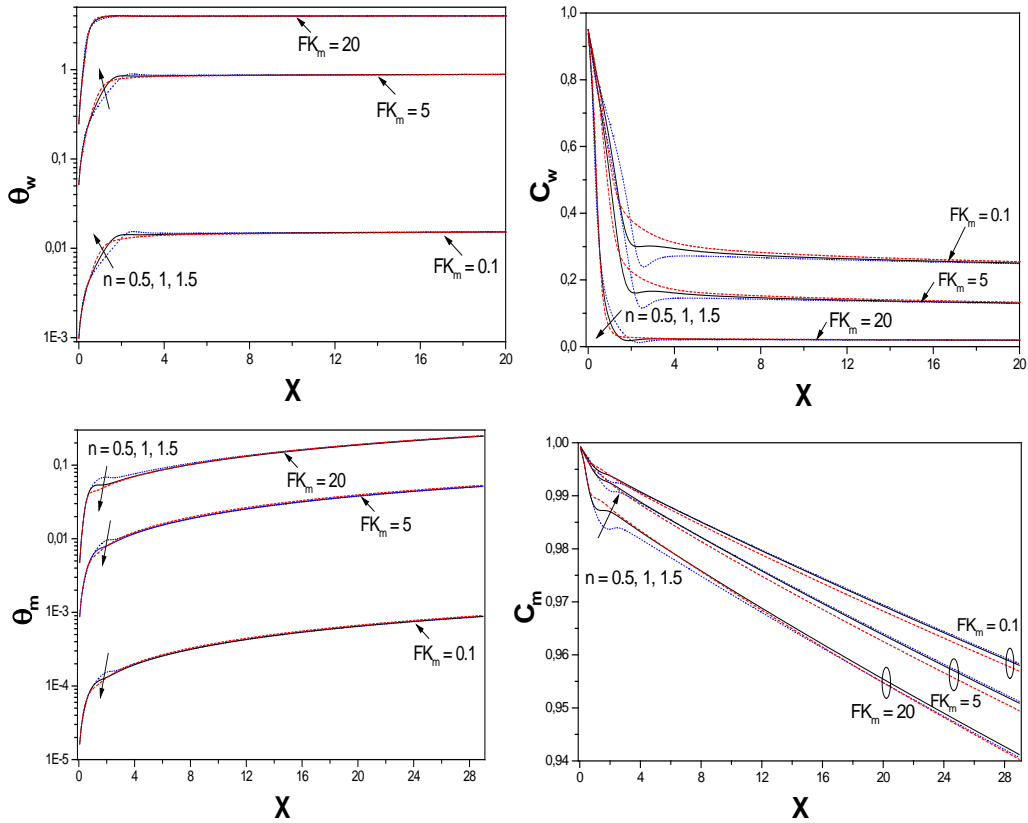


Figure 8: Variation of (θ_w, C_w) and (θ_m, C_m) with FK_m : $Da=10^{-3}$, $\lambda=1$ and $D_m=5$

The evolution of the mean Nusselt and Sherwood numbers with FK_m are presented on Fig. 9 which shows that the shear-thickening fluid exhibits the highest values of transfer rates, and that the exothermic nature of the chemical reaction becomes detrimental to heat and mass transfer only for a Frank-Kamenetskii number around 10 where Nu_m and Sh_m start to decrease.

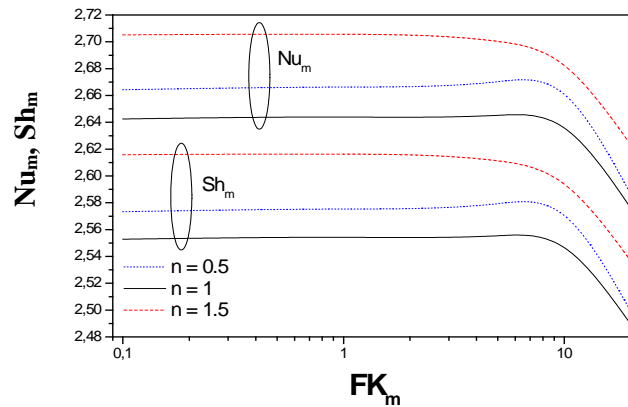


Figure 9: Variation of Nu_m and Sh_m with FK_m : $Da=10^{-3}$, $\lambda=1$ and $D_m=5$

The effect of the chemical reactivity, expressed by the modified Damköhler number, on the axial evolution of the temperature and concentration is illustrated on Fig. 10. As the Damköhler number represents the ratio between the time scales of diffusion and reaction, at high values of D_m the reaction gets faster and diffusion becomes dominant resulting in a reduction of θ_m and C_m as well as the parietal values θ_w and C_w where the effect of this parameter is more apparent since the reaction occurs on the channel walls. This situation leads to a decrease of heat and mass transfer rates with the modified Damköhler number as it appears in Fig. 11 where the highest values of Nu_m and Sh_m are obtained for a shear-thickening fluid.

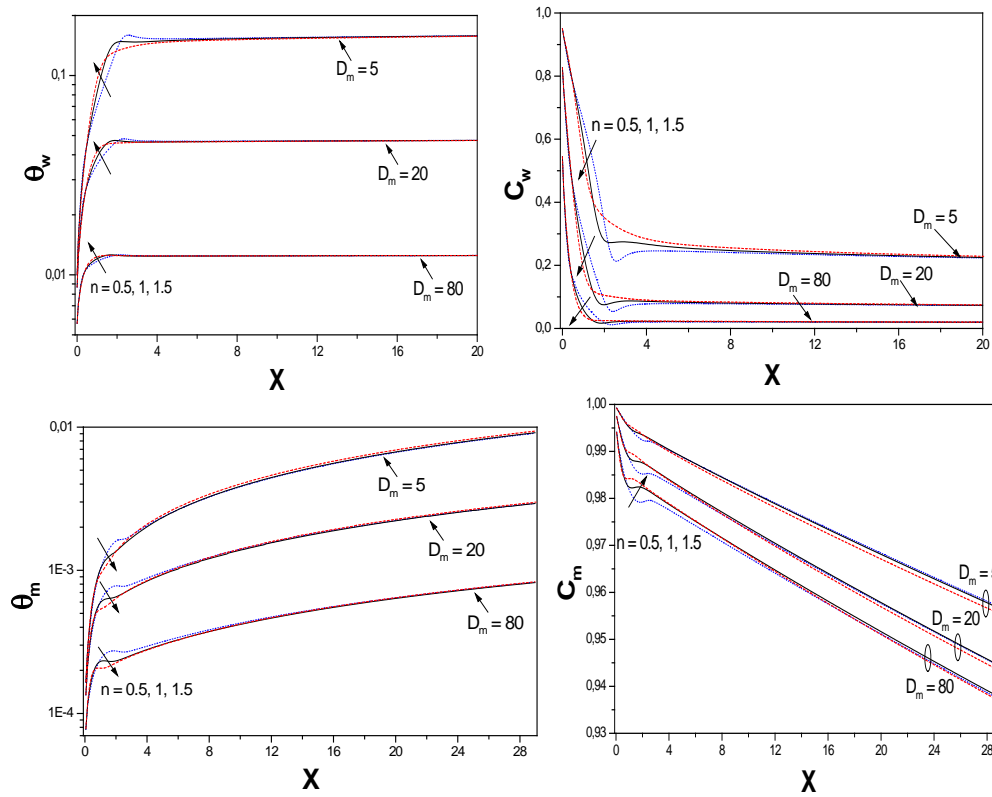


Figure 10: Variation of (θ_w, C_w) and (θ_m, C_m) with D_m : $Da=10^{-3}$, $\lambda=1$ and $FK_m=1$

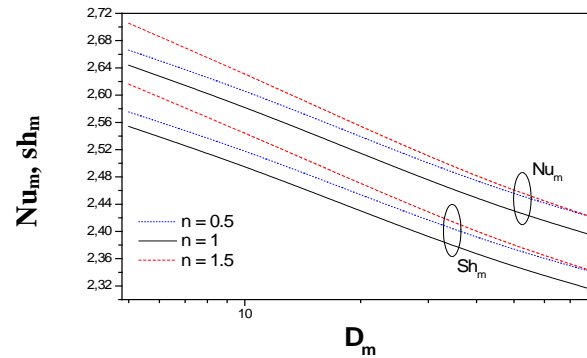


Figure 11: Variation of Nu_m and Sh_m with D_m : $Da=10^{-3}$, $\lambda=1$ and $FK_m=1$

5 Conclusion

Heat and Mass transfer of a power-law fluid with surface chemical reaction in a channel partly filled with an anisotropic porous medium are studied numerically. The effect of various parameters related to the porous medium (anisotropic ratio for thermal conductivity λ , and Darcy number Da), the non-Newtonian fluid (power-law index n), and the chemical reaction (modified Frank-Kamenetsii FK_m and modified Damköhler number D_m) on velocity, temperature and concentration distributions, as well as mean Nusselt and Sherwood numbers is analyzed. The parametric study allowed to highlights the following points:

- The augmentation of the anisotropic thermal conductivity ratio improves the heat transfer but decreases the mass transfer.
- At small Darcy number, the shear-thinning fluid exhibits the highest heat and mass transfer rates, and from a certain value of Da , which is strongly related to λ , it is the shear-thickening fluid which enhances the transfers.
- The comparison to the case of an isotropic porous medium reveals that thermal anisotropy affects strongly the exchanges. The highest gains on heat and mass transfer are obtained for $\lambda=10$ and $\lambda=0.1$ respectively. The maximum losses are achieved with $\lambda=0.1$ for heat transfer and with $\lambda=10$ for mass transfer. These values depend strongly on Da and n .
- The mean and wall temperatures and concentrations are strongly affected by the exothermic nature of the chemical reaction leading to a decrease of the heat and mass transfer rates with the augmentation of the modified Frank-Kamenetskii and Damköhler numbers.

Reference

Al-Nimr, M. A.; Aldoss, T. K. (2004): The effect of the macroscopic local inertial term on the non-Newtonian fluid flow in channels filled with porous medium. *International Journal of Heat & Mass Transfer*, vol. 47, pp. 125-133.

Alsabery, A. I.; Chamkha, A. J.; Hussain, S. H.; Saleh, H.; Hashim, I. (2015): Heatline visualization of natural convection in a trapezoidal cavity partly filled with nanofluid porous

layer and partly with non-Newtonian fluid layer. *Advanced Powder Technology*, vol. 26, pp. 1230-1244.

Amini, M.; Kafrudi, E. G.; Habibi M. R.; Ahmadi, A.; Nia, A. H. (2017): MHD flow and heat transfer of a magnetite-water nanofluid in porous medium under the effects of chemical reaction. *World Journal of Engineering*, vol. 14, pp. 193-199.

Bousri, A.; Bouhadef, K.; Langlet, T.; Beji, H. (2011): Forced convection analysis of coupled heat and mass transfer in a channel filled with a reactive porous medium. *Progress in Computational Fluid Dynamics*, vol. 11, pp. 305-317.

Chang, W. J.; Hsiao, C. F. (1993): Natural convection in a vertical cylinder filled with anisotropic porous media. *International Journal of Heat & Mass Transfer*, vol. 36, pp. 3361-3367.

Chen, G.; Hadim, A. (1998): Forced convection of a power-law fluid in a porous channel-numerical solution. *Heat & Mass Transfer*, vol. 34, pp. 221-228.

Chen, G. M.; Tso, C. P. (2011): Effects of viscous dissipation on forced convective heat transfer in a channel embedded in a power-law fluid saturated porous medium. *International Communications in Heat & Mass Transfer*, vol. 38, pp. 57-62.

Chen, Y. L.; Cao, X. D.; Zhu, K. Q. (2009): A gray lattice Boltzmann model for power-law fluid and its application in the study of slip velocity at porous interface. *Journal of Non-Newtonian Fluid Mechanics*, vol. 159, pp. 130-136.

Chikh, S.; Boumedien, A.; Bouhadef, K.; Lauriat G. (1995): Analytical solution of non-Darcian forced convection in an annular duct partially filled with a porous medium. *International Journal of Heat & Mass Transfer*, vol. 38, pp. 1543-1551.

Govender, S. (2006): On the effect of anisotropy on the stability of convection in rotating porous media. *Transport in Porous Media*, vol. 64, pp. 413-422.

Li, M.; Wu, Y.; Tian, Y.; Zhai, Y. (2007): Non-thermal equilibrium model of the coupled heat and mass transfer in strong endothermic chemical reaction system of porous media. *International Journal of Heat & Mass Transfer*, vol. 50, pp. 2936-2943.

Matin, M. H.; Pop, I. (2013): Forced convection heat and mass transfer flow of a nanofluid through a porous channel with first order chemical reaction on the wall. *International Communications in Heat & Mass Transfer*, vol. 46, pp. 134-141.

Minto, B. J.; Ingham, D. B.; Pop, I. (1998): Free convection driven by an exothermic reaction on a vertical surface embedded in porous media. *International Journal of Heat & Mass Transfer*, vol. 41, pp. 11-23.

Mobedi, M.; Cekmer, O.; Pop, I. (2010): Forced convection heat transfer inside an anisotropic porous channel with oblique principal axes: effect of viscous dissipation. *International Journal of Thermal Sciences*, vol. 49, pp. 1984-1993.

Moshizi, S. A. (2015): Forced convection heat and mass transfer of MHD nanofluid flow inside a porous microchannel with chemical reaction on the walls. *Engineering Computations*, vol. 32, pp. 2419-2442.

Nakayama, A.; Shenoy, A. V. (1993): Non-Darcy forced convective heat transfer in a channel embedded in a non-Newtonian inelastic fluid-saturated porous medium. *Canadian Journal of Chemical Engineering*, vol. 71, pp. 168-173.

Nebali, R.; Bouhadeb, K. (2006): Numerical study of forced convection in a 3D flow of a non-Newtonian fluid through a porous duct. *International Journal of Numerical Methods for Heat & Fluid Flow*, vol. 16, pp. 870-889.

Nebali, R.; Bouhadeb, K. (2011): Non-Newtonian fluid flow in plane channels: heat transfer enhancement using porous blocks. *International Journal of Thermal Sciences*, vol. 50, pp. 1984-1995.

Negara, A.; Salama, A.; Sun, S. (2015): Multiphase flow simulation with gravity effect in anisotropic porous media using multipoint flux approximation. *Computers & Fluids*, vol. 114, pp. 66-74.

Nithiarasu, P.; Sujatha, K. S.; Ravindran, K.; Sundarajan, T.; Seethramu, K. N. (2000): Non-Darcy natural convection in a hydrodynamically and thermally anisotropic porous medium. *Computer Methods in Applied Mechanics & Engineering*, vol. 188, pp. 413-430.

Patankar, S. V. (1980): *Numerical heat transfer and fluid flow*. McGraw-Hill, New York.

Postelnicu, A. (2009): Onset of convection in a horizontal porous layer driven by catalytic surface reaction on the lower wall. *International Journal of Heat & Mass Transfer*, vol. 52, pp. 2466-2470.

Shenoy, A. V. (1994): Non-Newtonian fluid heat transfer in porous media. *Advances in Heat Transfer*, vol. 24, pp. 101-190.

Zhang, J. Z.; Sun, R. Q. (1996): Non-Darcian and anisotropic effects on natural convection in horizontal porous media enclosure. *Journal of Thermal Science*, vol. 5, pp. 122-127.